Analysis of non-destructive testing ultrasonic signal for detection of defective materials based on the Simulink Matlab Mathematica computation method

Ade Febrianti*, Muhammad Hamdi, Juandi Muhammad

Department of Physics, Universitas Riau, Pekanbaru 28293, Indonesia

ABSTRACT

In this paper, an ultrasonic non-destructive test (NDT-UT) has been carried out on steel using the Simulink-MATLAB Mathematica computation method. This study aims to analyze the NDT-UT output signal for material defect detection using secondary data as the first sample. The sample is then analyzed using the fast Fourier transform (FFT) method to produce a spectrum waveform and image thermography. It can be seen that there is a decrease in signal height from 1 a.u to 0.55 a.u. The first sample waveforms were used to analyze the second sample, third sample, and fourth sample, and all the samples had different defects. The results of the sample analysis are in the form of a thermographic image that shows the temperature level based on the distribution of red (R), green (G), and blue (B) images on the sample surface. The NDT-UT output signal produces a sinusoidal wave similar to the results of the Simulink-MATLAB modeling analysis on the initial input echoes and the back wall, with a percentage inequality of 10%. Then validated the sinusoidal signal from the NDT-UT which gave a percentage of inequality between 0% – 42%. More complex or irregular defects result in a larger percentage or vice versa.

* Corresponding Author

E-mail address: adefebrianti89@gmail.com

1. INTRODUCTION

The rapid development of technology in the industrial sector has led to an increase in the use of industrial equipment. The use of industrial tools for a long period of time results in damage or defects in the form of corrosion, leakage, dislocation, and others. A defect is damage that interferes with or is detrimental to a certain structure during its use [1]. Preventive steps are needed to determine the condition of this industrial equipment so that we can find out what defects have occurred due to long-term use. Physical defects in solid objects, of course, cannot be known from direct sight, so it is necessary to carry out an inspection of an object to see whether or not there are defects that occur in solid objects [2]. Detection of defects and proper repair of micro defects are things that need to be done to prevent major defects and ensure the safety of all structural components [3]. This defect detection can be detected by conducting an inspection of the object or material. Inspections carried out in the industrial sector without damaging the solid objects being inspected are called non-destructive testing (NDT).

NDT is used primarily in the industrial world to detect defects, cracks, and voids in materials used in various structures with different types of materials [4]. In general, NTD has various methods, namely the ultrasonic test, penetrant test, radiography test, magnetic test, eddy current test [5]. One of the methods used is the non-destructive testing ultrasonic test (NDT-UT). NDT-UT is a test that is considered safe for use on various types of material and can reach the internal object being tested [6]. The working principle of the ultrasonic test method is to insert sound waves into the test specimen by vibrating each particle [7]. There are several previous studies using the NDT-UT method both nationally and internationally. Based on these previous studies, we need a method that can analyze the

NDT-UT output signal in the form of this image that can determine the location and shape of the defect to facilitate work in the field.

Image is an image that is recorded by the camera or by the sensor. The function of the image is a mathematical model that is often used by all analysis functions used to consider the image as a function with two variables [8, 9]. Image processing is carried out by transforming the input signal in the form of an image into an output image, either in the form of sinusoidal, histogram, or thermographic images. This image processing aims to improve the quality of the input image by using existing information and extracting an image using existing quantities so that the desired output image is produced in a better form. One of the digital signal processing methods applied to obtain the defect characteristics of the ultrasonic reflected signal is the Simulink-MATLAB Mathematica method. This technique can solve dynamic system simulations with differential equations and can design models using properties Simulink-MATLAB Mathematica. Simulink-MATLAB Mathematica equipped with examples of function systems. The function system provides a powerful mechanism for extending Simulation capabilities.

NDT-UT signal processing in the form of images using this Simulink-MATLAB Mathematica expected to save the production cost if using phased-array inspection is very expensive and the number of tools is inadequate, and there are few inspectors that can operate it. This is what makes the writer interested in conducting research with the title analysis of NDT-UT signals for defect detection in materials based on the Simulink-MATLAB Mathematica computing method. The purpose of this study is to analyze, reconstruct, and compare the reflected signal from the NDT-UT results with the results using the Matlab Simulink-Mathematica program. This research is limited to using secondary data from existing NDT-UT results.

2. THEORY

A defect in a structure can act as the start of a crack. Defects occur most likely during the crystal growth process or in the heat treatment process. This defect is divided into point defects, line defects, plane defects, and spatial defects. Defects that occur in metals cause damage to metal structures. This damage causes a decrease in the mechanical properties of the metal [10]. Physical defects in solid objects, of course, cannot be known from direct sight, so it is necessary to carry out an inspection of an object to see whether or not there are defects that occur in solid objects [2]. Detection of defects and proper repair of micro defects are things that need to be done to prevent major defects and ensure the safety of all structural components [3]. This defect detection can be detected by conducting an inspection of the object or material. Inspections carried out in the industrial sector without damaging the solid objects being inspected are called NDT.

NDT is a method of testing material to assess the characteristics of a component without changing or destroying the structure of the test material. NDT is very important in testing materials. This test can prove a defect in a hidden location. NDT uses the transmission of high-frequency sound waves to a material to detect defects and determine the location of the defects in a material. Generally, NDT has various methods, namely the ultrasonic test, penetrant test, the radiography test, the magnetic test, and Eddy current test [5]. However, this study uses secondary data from the ultrasonic test method. Ultrasonic testing is an inspection technique used to test various metal and metal products such as welded joints, forged objects, cast objects, thin sheets, tubes, plastics, and ceramics. The working principle is that the receiving wave in the form of an electronic device generates a high voltage and makes the transducer produce high frequency and ultrasonic waves. Ultrasonic waves enter the material and are reflected back towards the transducer before the propagation of these waves is displayed on the display. If there is a discontinuity, the wave will be reflected back and displayed on the display in the form of an image.

The image can be defined as a two-dimensional function in cartesian coordinates (x, y) which shows the relationship of image elements namely pixels and amplitude and each coordinate represents the smallest signal from the object. Pixel is a coordinate that represents the smallest signal from the image itself [11]. Image is also an image that is recorded by the camera or by the sensor. The function of the image is a mathematical model that is often used by all analysis functions used to consider the image as a function with two variables [8]. In theory, images are divided into three types, namely color images, grayscale images, and binary images. The color image is an image that has a pixel value and

can represent a certain color. The color image consists of three matrices representing the values of red (R), green (G), and blue (B). The redder the resulting color, the higher the temperature, and vice versa, the lower the temperature shown, the bluer the resulting color will be. In grayscale images, the image only consists of a red, gray, and white histogram, and has a depth of 8 bits or 256 gray color combinations so that the grayscale image only has one histogram [12]. Binary images are also called black and white images because they only have one pixel that needs to be represented by one bit of data. However, in terms of quality, it is not good because it only consists of two colors, namely black and white. The initial process that is mostly done in image processing is changing a color image to a grayscale image. This is used to simplify the image model [13]. There is a relationship between the color map and temperature as shown in the Table 1 [14].

Table 1. Range temperature such RGB color [14].

RGB color	(R, G, B) number	Grayscale number	Temperature range (°C)	Temperature average (°C)
	0, 0, 112	0 – 7	28.5 – 28.7	28.6
	0, 0, 153	8 – 15	28.8 – 29.0	28.9
	0, 0, 204	16 – 24	29.1 – 29.3	29.2
	0, 0, 255	25 – 33	29.4 – 29.6	29.5
	51, 51, 255	34 – 42	29.7 – 29.9	29.8
	0, 128, 255	43 – 51	30.0 – 30.2	30.1
	51, 153, 255	52 – 60	30.3 – 30.5	30.4
	51, 255, 255	61 – 69	30.6 – 30.8	30.7
	102, 255, 255	70 – 78	30.9 – 31.1	31.0
	153, 255, 255	79 – 87	31.2 – 31.4	31.3
	153, 255, 204	88 – 96	31.5 – 31.7	31.6
	102, 255, 178	97 – 105	31.8 – 32.0	31.9
	51, 255, 153	106 – 114	32.1 – 32.3	32.2
	51, 255, 51	115 – 123	32.4 – 32.6	32.5
	102, 255, 102	124 – 132	32.7 – 32.9	32.8
	153, 255, 153	133 – 141	33.0 – 33.2	33.1
	204, 255, 153	142 – 150	33.3 – 33.5	33.4
	178, 255, 102	151 – 159	33.6 – 33.8	33.7
	153, 255, 51	160 – 168	33.9 – 34.1	34.0
	255, 255, 51	169 – 177	34.2 – 34.4	34.3
	255, 255, 102	178 – 186	34.5 – 34.7	34.6
	255, 255, 153	187 – 195	34.8 – 35.0	34.9
	255, 204, 153	196 – 204	35.1 – 35.3	35.2
	255, 178, 102	205 – 213	35.4 – 35.6	35.5
	255, 102, 102	214 – 222	35.7 – 35.9	35.8
	255, 51, 51	223 – 231	36.0 – 36.2	36.1
	255, 0, 0	232 – 239	36.3 – 36.5	36.4
	204, 0, 0	240 – 247	36.6 – 36.8	36.7
	153, 0, 0	248 – 255	36.9 – 37.1	37.0

Based Table 1, it can be seen that the lowest temperature is 28.5°C with dark blue color, and the highest temperature is 37.1°C with dark red color. So it can be concluded that the false color indicates the redder the resulting color, the higher the temperature and vice versa, the lower the temperature shown, the bluer the resulting color will be.

Image processing is a process with input in the form of images and the results are also images. The results obtained from research using NDT-UT on the material in the form of digital images processed using Simulink-MATLAB Mathematica. Image processing has two main objectives in accordance with developments, namely [8]:
1. Improving image quality where the resulting image can display information clearly or in other words, humans can see the expected information by interpreting the existing image.
2. Extracting information that stands out in an image, namely general information where humans get characteristic information from the image numerically, or in other words, computers interpret the information in the image through clearly obtained data sizes.

Image processing operations can be classified into the following types [15]:

1. Image restoration, such as: removing blurring, the image looks blurry because the lens focus setting is not correct or the camera is moving and noise removal (noise).
2. Image compression, such as a 258 kb BMP image file compressed using the JPEG method to a size of 49 kb.
3. Image segmentation is closely related to pattern recognition.
4. Image analysis, such as image edge detection.
5. Image reconstruction, such as some X-rays are used to form bone images of body organs.

The operation carried out in this study is to analyze the image segmentation, then analyze the NDT-UT resulting image on the material which contains several existing defects. And then reconstructed using Mathematica so that we know the shape of the defects that occur in the material. MATLAB is a programming language that can help solve various mathematical problems that are often encountered in the technical field. MATLAB integrates computing, visualization, and programming in a user-friendly model where problems and their solutions are expressed in familiar notation. MATLAB is a numerical computing environment and fourth-generation computer programming language. MATLAB has the following characteristics [16]:

1. The programming language is based on a matrix (rows and columns).
2. There are many toolboxes for special applications, such as Simulink, neural network, state flow, data acquisition toolbox, communications block set, fuzzy logic toolbox, image acquisition toolbox, signal processing block set, and so on.
3. In writing the code, you don't have to declare the array first.
4. Has a faster development time compared to traditional programmings such as Fortran and C.

One of the toolboxes for applications in MATLAB is Simulink. Simulink is a visual program designed to create an intuitive modeling system that provides a way to solve equations numerically using graphics, rather than using code [17]. Signal analysis in Simulink-MATLAB uses fast Fourier transform (FFT) filters to produce a waveform, wave spectrum, and thermographic image. The working principle of FFT is to divide the sampled signal into several parts, then each part is completed with the same algorithm and the results are collected again [18]. The advantage of FFT is that it is able to show the frequency content contained in the signal and is able to show several frequency components that are in the signal. Meanwhile, the weakness that FFT has is that it is only able to analyze stationary cues while there are many non-stationary cues and only provides information in the form of all the frequency content contained in the signal, but cannot show the time of occurrence of these frequencies simultaneously [15].

Wolfram Mathematica has specifications for numerical, algebraic, graphical, and various other forms. The concept of Wolfram Mathematica is to make one or all systems able to handle various aspects of computational techniques in a coherent and integrated manner. So that it can manipulate various objects that exist in computational techniques using only a few basic primitives [19, 20]. So that Wolfram Mathematica can be used to analyze images. To remove noise in the image, a Gaussian filter is used. The Gaussian filter is very good at removing noise that is normally distributed, which is often found in the distribution of images from the digitizing process using a camera because it is a natural phenomenon due to the nature of light reflection and the sensitivity of the light sensor on the camera itself [21]. Gaussian filters are operators that are usually used to obscure or remove noise [22]. This process is useful for smoothing an image that appears slightly blurry and for producing true edges of the image. Noise is a form of damage to the signal display caused by external interference. Disturbance in the image is generally in the form of a pixel intensity that is not correlated with neighboring pixels [23].

3. RESEARCH METHODS

The research method was carried out computationally using MATLAB software with the Mathematica-Simulink modeling program. The tools and materials used in the study to analyze NDT-UT signals, namely Laptop Hp 100-1441TU, MATLAB-Simulink software, Wolfram Mathematica, and NDT-UT signals (secondary data).
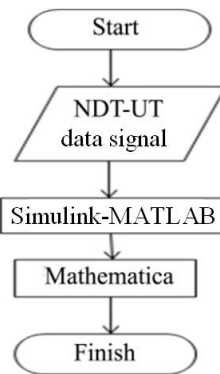
Figure 1. The NDT-UT signal analysis research flowchart.

The programming flow is shown in Figure 1. The input data is in the form of NDT-UT signal data from the experiment which is then analyzed using MATLAB Simulink-Mathematica to produce waveforms and thermographic images which are finally refined using Mathematica to get 3D results. The research procedure is shown in Figure 2.
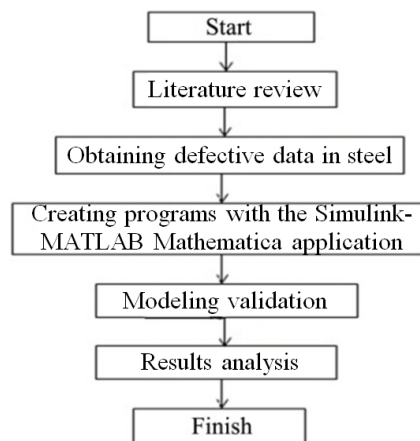
Figure 2. The procedure of this research.

The data used in this study are sample 1 (experimental data using a modified sample in such a way, sample 2 (empty black space depicted in 3D visual zoom), sample 3 (steel plate material that has a surface with irregular defects.), and sample 4 (modified defect shape with wave-shaped crack). The program used to analyze the NDT-UT signal for defect detection is Mathematica-Simulink. One of the functions in Mathematica-Simulink is to plan the 3D surface parametrically.
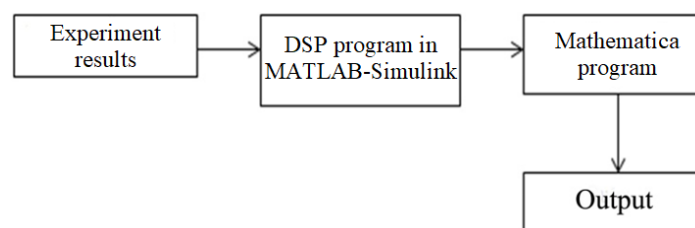
Figure 3. The Simulink- MATLAB Mathematica system diagram.

Simulink designs are transformed into Mathematica through the Mathematica-Simulink program with modified Mathematica graphics as shown in Figure 3. The Mathematica-Simulink program is applied to analyze a Simulink-based dynamic system with a model built through analog circuit steps.
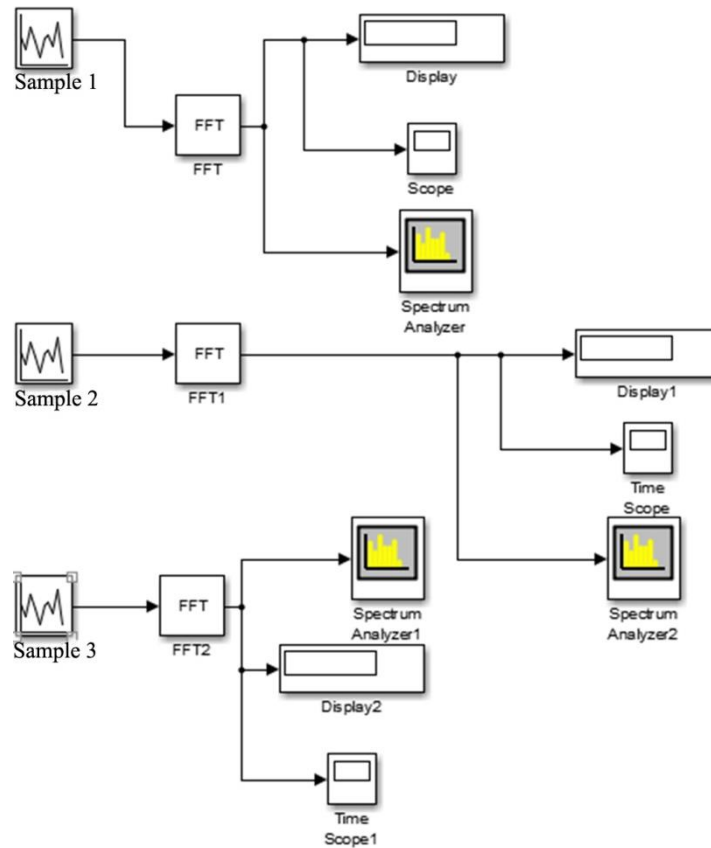
Figure 4. The control loop for the defect detection NDT-UT output signal.

Figure 4 shows the series of defect detection processes for all samples. Sample 1, sample 2, and sample 3 are experimental data using NDT-UT. The data will then be processed through the FFT so that it is transformed to produce an output in the form of a waveform, spectrum distribution, and thermographic image. These results will then be analyzed using the Mathematica program to produce a 3D view. The program that has been made is validated to see the accuracy and percentage error of the experimental literature by comparing the effect of the impedance of air and steel on the sinusoidal shape of the samples used.

4. RESULTS AND DISCUSSION

The Secondary data used in this study were taken from experimental data on defect detection in steel materials using NDT-UT. The data is in the form of reading data from an oscilloscope which has a data length of 4000 with a sampling frequency of 100 MHz. Secondary data is designated as sample 1 in this study.
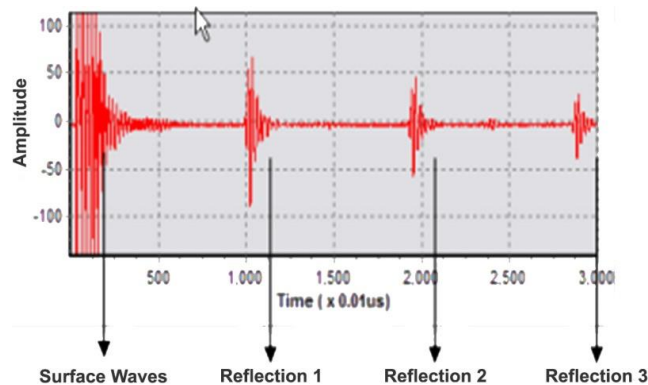
Figure 5. Ultrasonic reflection signal.

Based on Figure 5, the first waves that appear are ultrasonic vibrations on the surface. Followed by reflected waves 1, 2, and 3. From the first reflected wave to the 2nd and 3rd reflected waves attenuation by 20% of the signal. Frequency energy appears at a frequency of 4.42 MHz [4]. Based on the results of the experiment, the following waveforms are obtained in Figure 6 (a).
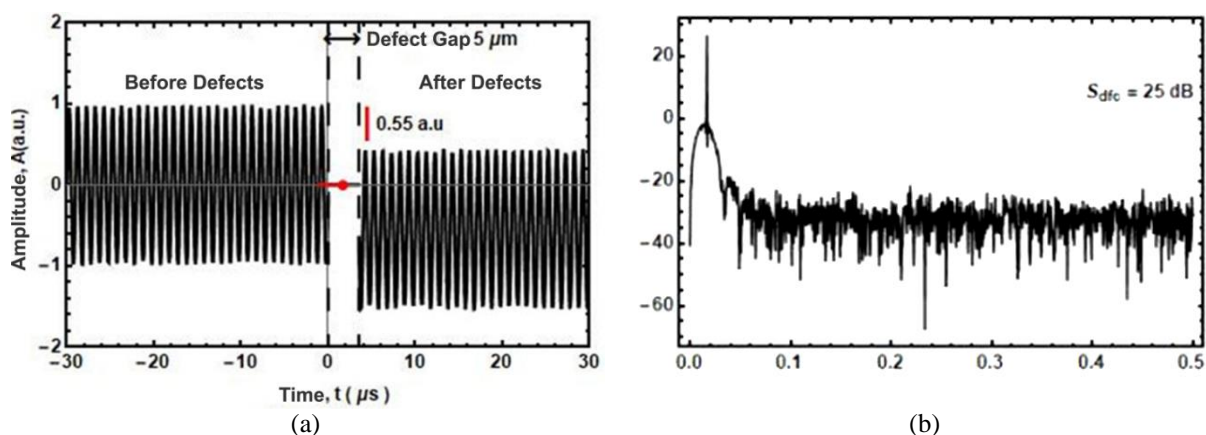
Figure 6. Waveforms results: (a) experiment; and (b) distribution of the power spectrum.

The magnitude of the wave amplitude on the surface before hitting the defect surface is 1 a.u. After passing through the defect gap measuring 5 μm, it is seen that there is a decrease in the amplitude from 1 a.u to 0.55 a.u as shown in Figure 6 (a) and (b). This decrease is because only part of the energy from the wave is reflected back from the defective surface. If there is a discontinuity, the waves will be reflected back and displayed on the display [24]. The waveform is then processed using a FFT. FFT is used to transform a signal from the time domain into a frequency signal. FFT is able to show the frequency content contained in the signal and show how many frequency components are in the signal [25]. So that the resulting sample frequency distribution 1 is as follows. The Figure 6 (b) shows the distribution of the power spectrum in sample 1, so that there is a decrease in the power spectrum from 25 dB to between -20 dB to -75 dB. This decrease occurs when the wave after hitting the defective surface in sample 1, the highest power spectrum produced is 25 dB. Image processing aims to improve image quality so that it is easily interpreted by humans or computers [26].

In the frequency domain method, the processing technique is based on the Fourier transform using FFT to the pixel value in the form of a thermographic image histogram graphic. An image histogram is a graphic depicting the distribution of pixel intensity values from an image or a certain part of the image. Figure 7 (a) shows the color distribution in the resulting thermographic image. This thermographic image displays a color image of sample 1 used. In a color image, each point has a specific color which is a combination of 3 basic colors, each color directed to one of the hardware standards (RGB, CMY, YIQ) or image processing applications [27]. Based on the relationship between the color map and the temperature of the image. Thermography shows the temperature distribution according to the existing color combinations. The red color on the thermographic image shows the highest temperature level (35.7°C – 37.1°C), yellow color indicates the temperature is 34.1°C – 35°C, and the green color indicates the temperature between 31.5°C – 34.1°C. While the blue color shows the temperature between 28.5 °C – 30.5 °C. Based on the temperature distribution, it can be seen that there is an orderly temperature distribution on the thermographic image. There is a red color in the slit of the thermographic image which shows the highest temperature so that it indicates a defect in the area caused by a difference in thickness in that area. This corresponds to the shape of sample 1 which has an empty gap in the middle. In addition, a significant decrease in amplitude can be seen at a position between -25 pixels to -20 pixels. This corresponds to the shape of sample 1 which has an empty gap in the middle. In addition, a significant decrease in amplitude is seen at positions between -25 pixels to -20 pixels. This corresponds to the shape of sample 1 which has an empty gap in the middle. In addition, a significant decrease in amplitude can be seen at a position between -25 pixels to -20 pixels.
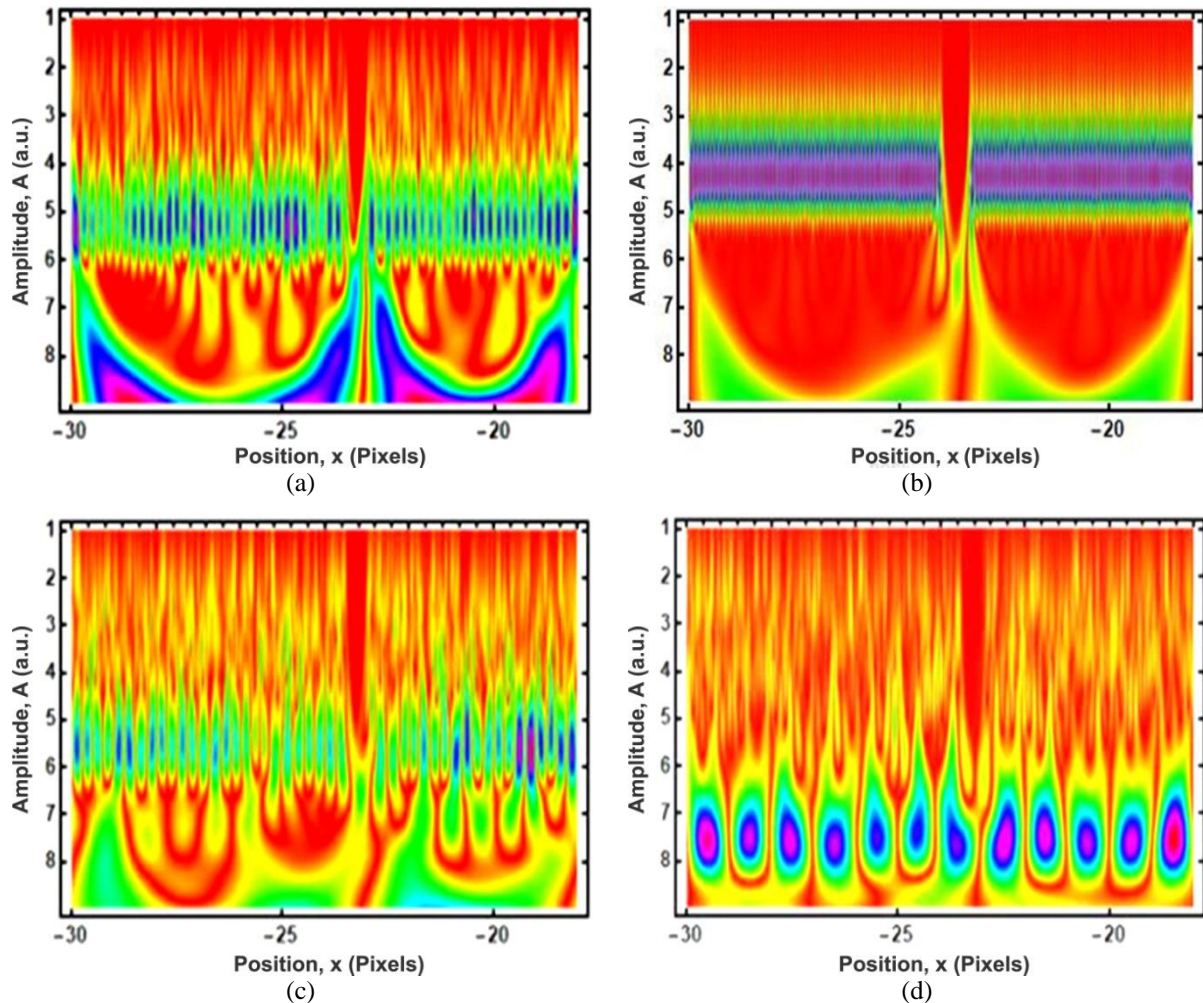
(a)

(b)

(c)

(d)

Figure 7. Image results: (a) color distribution in thermographic image; (b) quite a lot of red distribution; (c) irregular distribution of the RGB color; and (d) distribution of RGB colors.

By using the waveform sample 1, an analysis was carried out on sample 2 whose defective shape in the form of empty black space is depicted visually zoom it looks like a block for 3D but uses 1D inner lines and a 2D piece of board. Then the processing is carried out using Simulink-MATLAB, resulting in a thermographic image as shown in Figure 7 (b), shows that there is quite a lot of red distribution in the resulting thermographic image. The color image produced in this thermographic image has a very regular distribution of red, green, yellow, and blue colors. Each color has a different temperature level, this depends on the thickness of the object. The red color indicates a very high temperature, thus indicating a defect in the object. This is in accordance with the shape from sample 2 used because sample 2 has a defective shape in the form of an empty black space depicted in a visual zoom like a block for 3D but uses lines in 1D and a 2D board. In addition, there is a decrease in amplitude at a position between -25 pixels to -20 pixels.

By using the waveform sample 1, an analysis was carried out on sample 3 with a defect in the form of an irregular surface. The results of the MATLAB-Simulink analysis in sample 3 obtained a display in thermographic form as follows in Figure 7 (c), shows the irregular distribution of the RGB color of the resulting thermographic image. You can see a red distribution which indicates a high-temperature level and indicates a defect in the area. This is consistent with the form from sample 3 which used an irregular shape of the surface defect. In addition, there is a decrease in wave amplitude due to the defective surface in sample 3. A very significant decrease is seen at the position between -25 pixels to -20 pixels.

By using the waveform sample 1, an analysis was carried out on sample 4 with a defect in the form of a wave-shaped crack. Results of the analysis MATLAB-Simulink In sample 4, the display in

thermographic form is obtained as follows in Figure 7 (d), shows the distribution of RGB colors in the resulting thermographic image. The shape of this thermographic image looks quite regular with red appearing around certain parts. This means that there is a high temperature in certain parts that indicate a defect in the area. This corresponds to the shape of sample 4 in the form of a wave-shaped crack. In addition, there is a decrease in amplitude in some parts of the sample due to waves hitting the defect surface, resulting in a light-dark image according to the shape of the defect used.

Based on the experimental results from detecting defects in the material using NDT-UT which is then analyzed using a program Simulink-MATLAB so that the resulting image display in the form of thermography of each sample. This thermographic image is ultimately reprocessed using the Wolfram Mathematica program to produce a 3D view. Image processing has improved the quality of the resulting image by interpreting existing images and extracting existing information through existing data volumes [8]. By using the Wolfram Mathematica program to analyze the input image in the form of a thermographic image generated from Simulink-MATLAB, 3D views are generated for each sample which can be seen in the following pictures.
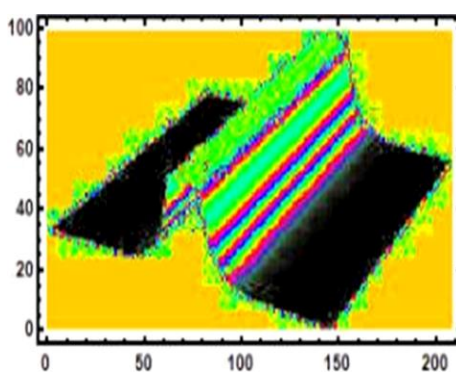
Figure 8. The 3D shape of sample 1.

Figure 8 shows the 3D shape of sample 1 in the form of a defect with a deep curve in the center. This corresponds to the shape of the defect used in sample 2. However, the results obtained are not of very good quality, this is due to the irregular frequency of the waves used so that it affects the results of the 3D display.
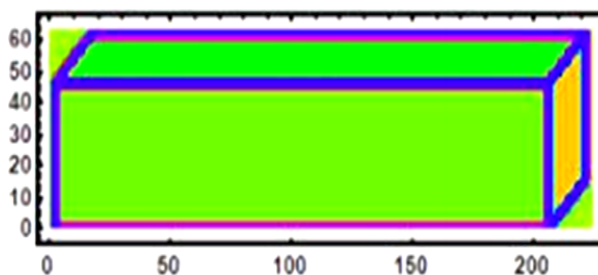
Figure 9. The shape of sample 2.

Figure 9 shows the shape of sample 2 in the form of a block. This corresponds to the deformed shape of a blank black space depicted in a visual zoom like a block for 3D but using 1D inner lines and a 2D piece of board.

Figure 10 (a) shows the 3D view produced after being processed using the Simulink-MATLAB Mathematica model so that you can see the shape of the defects that occur. However, the resulting 3D view is not very clear due to the irregular and complex frequency of the waves used. This results in the display results that are less clear. Figure 10 (b) shows the resulting 3D view after processing using Simulink-MATLAB Mathematica. So that you can see the shape of the defects that occur. However, because sample 4 uses an irregular frequency with a defective shape in the form of a circular wave, the quality of the 3D display is not very clear.

Figure 10. the 3D view produced after being processed using the Simulink Matlab-Mathematica: (a) less clear and (b) very clear.

Based on the reflected waveform generated from the experiment using NDT-UT the first reflected wave is produced as follows in Figure 11. The Figure 11 (a) shows that the maximum height at the A1 position is 1 a.u, while at the S1 position the maximum height is 0.55 a.u, there is a decrease in the amplitude from the initial entry to the back wall echo, this is due to an indication of the paint that occurs in that area. In accordance with the working principle of ultrasoni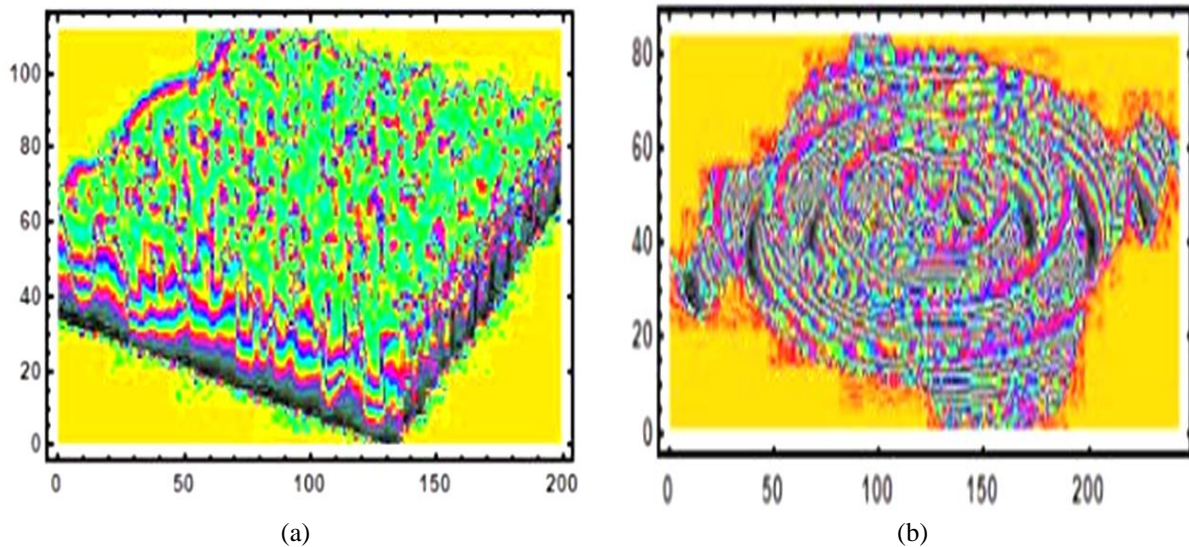c testing, namely a decrease in wave frequency due to discontinuities that occur in the material [24]. Then compared with the results from Simulink-MATLAB as shown in the Figure 11 (b) is a waveform as a result of analysis using Simulink-MATLAB. At the A1 position, you can see that the maximum height generated is close to 1 a.u, which is 0.9 a.u, while in the S1 position you can see the maximum height produced is 0.5 a.u so that there is a decrease in the amplitude seen in the resulting reflected wave. This is due to discontinuities or defects in the sample material used.
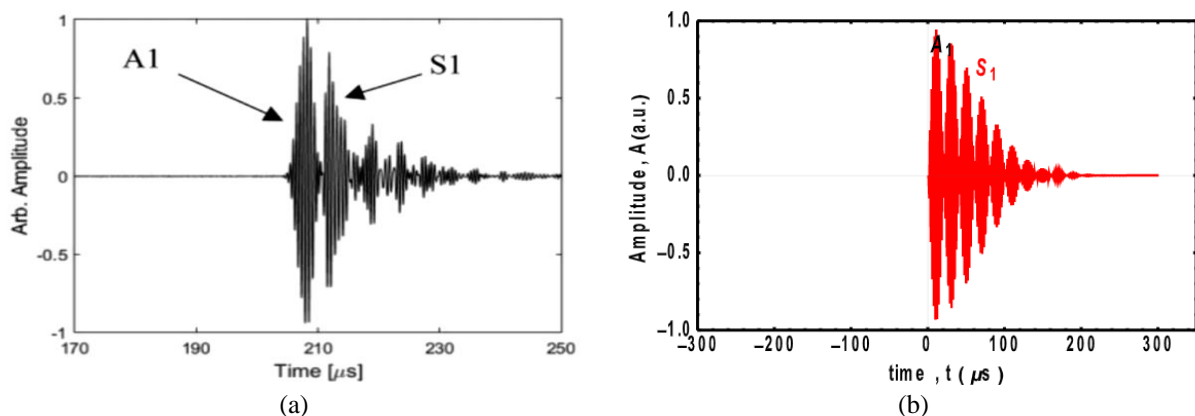
Figure 11. Reflected waveform generated using: (a) NDT-UT and (b) Simulink-MATLAB.

Based on Figure 11 (a) and (b), it can be seen that there is a similarity in waveforms in A1 and S1 resulting from experiments and analysis results using Simulink-MATLAB. At position A1, which is a condition called initial entry, the results of the experiment resulted in a maximum height of 1 a.u, while the maximum height generated from the analysis using Simulink-MATLAB is 0.9 a.u. the percentage of inequality is 10%.

In addition, validation for this study was carried out by looking at the comparison of the sinusoidal form of the NDT-UT results for each sample of air and steel. It is known that there is a

difference in the impedance of air and steel, steel has an impedance of 46.1×10^6 kg/m^{2}s. Meanwhile, the air has an impedance of 413 kg/m^{2}s [28]. Acoustic impedance is required in determining the acoustic transmission and reflection limits of two materials having different acoustic impedances, ultrasonic transducer design, and pen rating absorption of sound in a medium m^{2}s [28].

Figure 12 (a) is a sinusoidal view of sample 1 with defects modified in such a way as to form letters, it can be seen that the maximum height of the waves in the air is 450 volts, while the maximum height of the waves in steel is 350 volts. So the percentage level of inequality is 22.22%. Figure 12 (b) is a sinusoidal view of sample 2 with a defect in the form of empty black space depicted in a 3D visual zoom. You can see that the maximum height of the waves in the air is 400 volts, while the maximum height of waves in steel is 400 volts. So the percentage level of inequality is 0%. Figure 12 (c) is a sinusoidal view of sample 3 in the form of a steel material plate that has a surface problem with irregular defects, you can see that the maximum height of the waves in the air is 2.6 a.u, while the maximum height of the waves in steel is 1.1 a.u. So that the percentage level of inequality is 42.11%. Figure 12 (d) is a sinusoidal view of a sample of 4 modified defects with wave-shaped cracks, it can be seen that the maximum height of the waves in the air is 25 dB, while the maximum height of the waves in steel is 22 dB. So the percentage level of inequality is 12%. Based on Figure 12, it can be concluded that the shape of the defect used affects the magnitude of the percentage of errors that occur. The more complex the shape of the defect that occurs, the greater the percentage of inequality that occurs, namely 42% with irregular defects across the surface of the sample. Likewise, on the contrary, the higher the level of defect regularity used, the smaller the percentage of inequality that occurs, namely 0%.
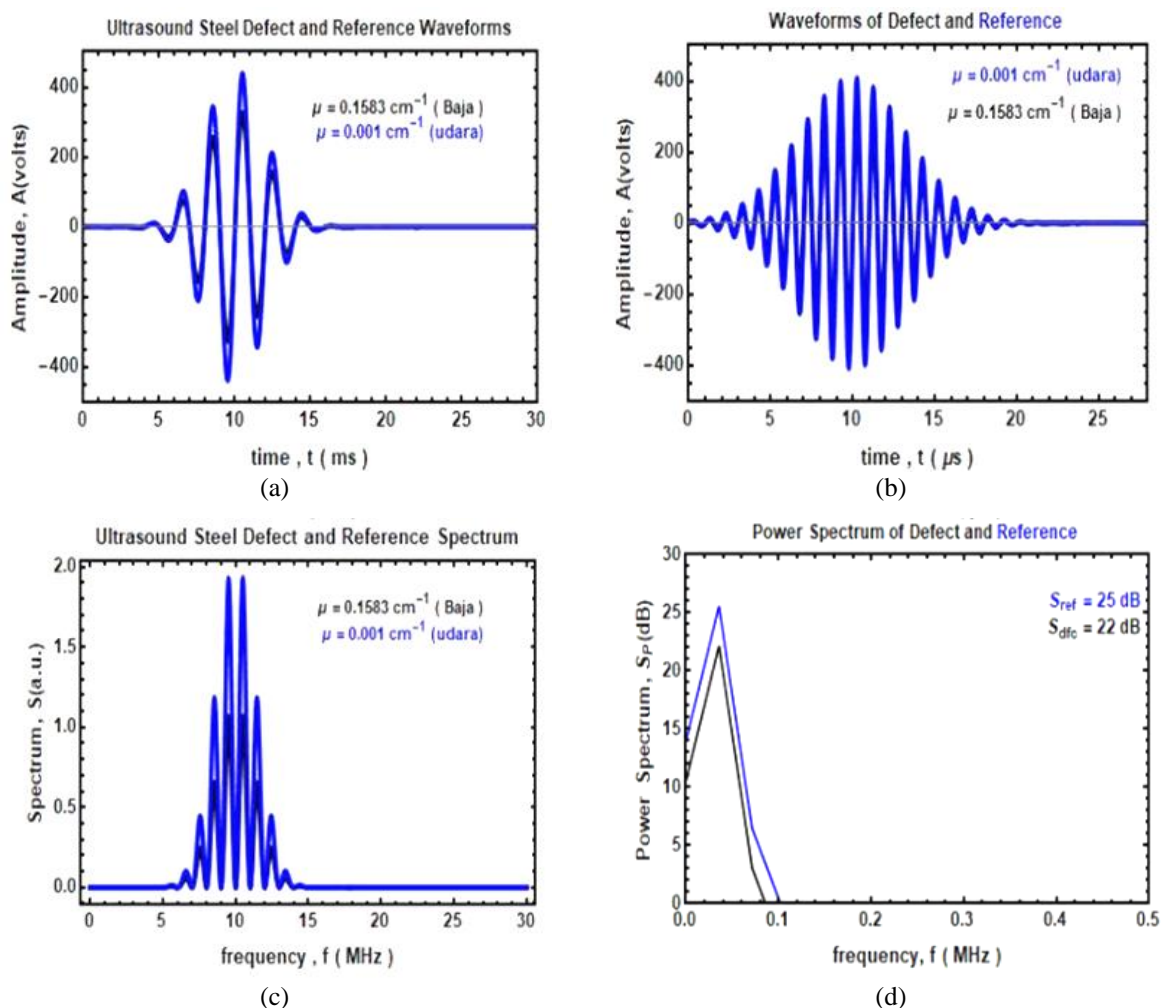

Figure 12. Sinusoidal wave: (a) sample 1 with defects modified; (b) sample 2 with a defect; (c) sample 3 in the form of a steel material; and (d) sample of 4 modified defects.

5. CONCLUSION

The MATLAB-Simulink Mathematica program can analyze the output signal generated and displayed on the CRT screen from the experimental results using the NDT-UT. It can be seen that there are similarities in the waveform, power spectrum distribution, and thermographic image in each sample with the sample shape used. In sample 1, there was a decrease in the maximum wave height from 1 a.u to 0.55 a.u. This is also seen in the frequency distribution of the sample 1 signal which decreased from 25 dB to -75 dB, which was due to discontinuities that occurred in the sample. In the thermographic image, the RGB distribution is shown according to the form of the defect used. The distribution of red, green, and indicates the level of temperature that occurs on the surface of the object. The Simulink-MATLAB Mathematica program can reconstruct in 3D using experimental data on the defect samples used so that the shape and position of the defect can be seen. The resulting image has a quality that is not so clear depending on the shape of the defect sample frequency used. The more complex the frequency used, the less clear the image is produced. The results obtained from the output signal using the NDT-UT in the form of a sinusoidal wave are similar to the results of the analysis using the Simulink-MATLAB modeling program. The experimental results for the maximum height of the amplitude at the core entry were 1 a.u, while the Simulink-MATLAB analysis resulted in 0.9 a.u. the inequality of the resulting reflected wave is 10%. Validation is done by comparing the sinusoidal output shape of the NDT-UT of each sample against air and steel in the presence of differences in impedance of steel and air. The shape of the defect used affects the size of the error presentation. The more complex the shape of the defect that occurs makes the percentage of inequality that occurs is as large as 42% with an irregular shape of the defect across the sample surface. Conversely, the higher the defect regularity used, the smaller the percentage of inequality that occurs, namely 0%.

REFERENCES

[1] Remillieux, M. C., Kaoumi, D., Ohara, Y., Geesey, M. A. S., Xi, L., Schoell, R., Bryan, C. R., Enos, D. G., Summa, D. A., Ulrich, T. J., Anderson, B.E., & Shayer, Z. (2020). Detecting and imaging stress corrosion cracking in stainless steel, with application to inspecting storage canisters for spent nuclear fuel. *NDT and E International*, **109**, 102180.

[2] Angjeliu, G., Coronelli, D., & Cardani, G. (2020). Development of the simulation model for Digital Twin applications in historical masonry buildings: The integration between numerical and experimental reality. *Computers and Structures*, **238**, 106282.

[3] Taheri, H., Shoaib, M. R. B. M., Koester, L. W., Bigelow, T. A., Collins, P. C., & Bond, L. J. (2017). Powder-based additive manufacturing-a review of types of defects, generation mechanisms, detection, property evaluation and metrology. *International Journal of Additive and Subtractive Materials Manufacturing*, **1**(2), 172–209.

[4] Farhana, N. I. E., Majid, M. A., Paulraj, M. P., Ahmadhilmi, E., Fakhzan, M. N., & Gibson, A. G. (2016). A novel vibration based non-destructive testing for predicting glass fibre/matrix volume fraction in composites using a neural network model. *Composite Structures*, **144**, 96–107.

[5] Sorger, G. L., Oliveira, J. P., Inácio, P. L., Enzinger, N., Vilaça, P., Miranda, R. M., & Santos, T. G. (2019). Non-destructive microstructural analysis by electrical conductivity: Comparison with hardness measurements in different materials. *Journal of materials science & technology*, **35**(3), 360–368.

[6] Acevedo, R., Sedlak, P., Kolman, R., & Fredel, M. (2020). Residual stress analysis of additive manufacturing of metallic parts using ultrasonic waves: State of the art review. *Journal of Materials Research and Technology*, **9**(4), 9457–9477.

[7] Grager, J. C., Kotschate, D., Gamper, J., Gaal, M., Pinkert, K., Mooshofer, H., Goldammer, M., & Grosse, C. U. (2018). Advances in air-coupled ultrasonic testing combining an optical microphone with novel transmitter concepts. *12th European conference on Non-Destructive Testing*, ECNDT-0166.

[8] Sheykhmousa, M., Mahdianpari, M., Ghanbari, H., Mohammadimanesh, F., Ghamisi, P., & Homayouni, S. (2020). Support vector machine versus random forest for remote sensing image

classification: A meta-analysis and systematic review. *IEEE Journal of Selected Topics in Applied Earth Observations and Remote Sensing*, **13**, 6308–6325.

[9] Yani, R. A., Saktioto, S., & Husein, I. R. (2020). Volumetric Prediction of Symmetrical-Shaped Fruits by Computer Vision. *Science, Technology & Communication Journal*, **1**(1), 20–26.

[10] Ahmadi, A., Mirzaeifar, R., Moghaddam, N. S., Turabi, A. S., Karaca, H. E., & Elahinia, M. (2016). Effect of manufacturing parameters on mechanical properties of 316L stainless steel parts fabricated by selective laser melting: A computational framework. *Materials and Design*, **112**, 328–338.

[11] Feinstein, A. D., Montet, B. T., Foreman-Mackey, D., Bedell, M. E., Saunders, N., Bean, J. L., Christiansen, J. L., Hedges, C., Luger, R., Scolnic, D., & de Miranda Cardoso, J. V. (2019). eleanor: An open-source tool for extracting light curves from the TESS Full-Frame Images. *Publications of the Astronomical Society of the Pacific*, **131**(1003), 094502.

[12] Kurniastuti, I., Wulan, T. D., Purnama, I. K. E., & Purnomo, M. H. (2017). Perbaikan citra x-ray gigi menggunakan contrast stretching. *Technology Science and Engineering Journal*, **1**(1), 8–13.

[13] Huang, D., Wang, Y., Song, W., Sequeira, J., & Mavromatis, S. (2018). Shallow-water image enhancement using relative global histogram stretching based on adaptive parameter acquisition. *MultiMedia Modeling: 24th International Conference, MMM 2018, Bangkok, Thailand, February 5-7, 2018, Proceedings, Part I*, **24**, 453–465.

[14] Budiarti, P. W. (2016). *Analisis thermal signature wajah manusia pada saat aktifitas jogging dengan teknik termografi inframerah*, Doctoral dissertation, Institut Teknologi Sepuluh Nopember.

[15] Alfaro-Almagro, F., Jenkinson, M., Bangerter, N. K., Andersson, J. L., Griffanti, L., Douaud, G., Sotiropoulos, S. N., Jbabdi, S., Hernandez-Fernandez, M., Vallee, E., Vidaurre, D., Webster, M., McCarthy, P., Rorden, C., Daducci, A., Alexander, D. C., Zhang, H., Dragonu, I., Matthews, P. M., Miller, K. L., & Smith, S. M. (2018). Image processing and Quality Control for the first 10,000 brain imaging datasets from UK Biobank. *Neuroimage*, **166**, 400–424.

[16] Cui, Q., Liang, K., Gao, H., Chen, G., Wang, N., Jin, S., Zhong, C., Cui, S., Sun, D., Fang, J., Han, C., Xu, B., An, Y., & Xu, M. (2016). Research of the transformer fault diagnosis expert system based on esta and deep learning neural network programmed in MATLAB. *2016 International Conference on Civil, Transportation and Environment*, 772–778.

[17] Lv, M., Li, Y., Liu, W., Guo, R., Yang, L., Pang, L., Li, Y., & Wang, J. (2016). Development of simulation platform for physicochemical regenerative environment control and life support system in space station. *2016 IEEE 11th Conference on Industrial Electronics and Applications (ICIEA)*, 1145–1150.

[18] Ferreira, V. H., Zanghi, R., Fortes, M. Z., Sotelo, G. G., Silva, R. D. B. M., Souza, J. C. S., Guimarães, C. H. C., & Gomes Jr, S. (2016). A survey on intelligent system application to fault diagnosis in electric power system transmission lines. *Electric Power Systems Research*, **136**, 135–153.

[19] Noack, M., Reinefeld, A., Kramer, T., & Steinke, T. (2018). Dm-heom: A portable and scalable solver-framework for the hierarchical equations of motion. *2018 IEEE International Parallel and Distributed Processing Symposium Workshops (IPDPSW)*, 947–956.

[20] Zairmi, Y., Veriyanti, V., Candra, W., Syahputra, R. F., Soerbakti, Y., Asyana, V., Irawan, D., Hairi, H., Hussein, N. A., & Anita, S. (2020). Birefringence and polarization mode dispersion phenomena of commercial optical fiber in telecommunication networks. *Journal of Physics: Conference Series*, **1655**(1), 012160.

[21] Malik, U., Krisman, K., Syech, R., & Hamdi, M. (2018). Heat transfer and mapping of THz radiation absorption in biological tissue using Mathematica based Simulink transform. *Malaysian Journal of Fundamental and Applied Sciences*, **14**(4), 500–508.

[22] Mafi, M., Martin, H., Cabrerizo, M., Andrian, J., Barreto, A., & Adjouadi, M. (2019). A comprehensive survey on impulse and Gaussian denoising filters for digital images. *Signal Processing*, **157**, 236–260.

[23] Kurukuru, V. B., Haque, A., & Khan, M. A. (2019). Fault classification for photovoltaic modules using thermography and image processing. *2019 IEEE Industry Applications Society Annual Meeting*, 1–6.

[24] Pitalokha, R. A., Mulyana, C., Hamdani, M. R., & Muhammad, F. (2016). Inspeksi cacat (diskontinuitas) pada material dengan menggunakan uji ultrasonik dan uji radiografi. *Prosiding Seminar Nasional Fisika (E-Journal)*, **5**, SNF2016-MPS.

[25] de Jesus Romero-Troncoso, R. (2016). Multirate signal processing to improve FFT-based analysis for detecting faults in induction motors. *IEEE Transactions on industrial informatics*, **13**(3), 1291–1300.

[26] Xing, F., Xie, Y., Su, H., Liu, F., & Yang, L. (2017). Deep learning in microscopy image analysis: A survey. *IEEE Transactions on Neural Networks and Learning Systems*, **29**(10), 4550–4568.

[27] Kahu, S. Y., Raut, R. B., & Bhurchandi, K. M. (2019). Review and evaluation of color spaces for image/video compression. *Color Research and Application*, **44**(1), 8–33.

[28] Hijazi, A. & Kähler, C. J. (2017). Contribution of the imaging system components in the overall error of the two-dimensional digital image correlation technique. *Journal of Testing and Evaluation*, **45**(2), 369–384.